

Dynamic light storage based on controllable electromagnetically induced transparency effect

Liu-Ying Zeng(曾柳莹), Jun-Fang Wu(吴俊芳), and Chao Li(李潮)

Citation: Chin. Phys. B, 2023, 32 (**6**): 064213. DOI: 10.1088/1674-1056/acd2bd
Journal homepage: http://cpb.iphy.ac.cn; http://iopscience.iop.org/cpb

What follows is a list of articles you may be interested in

Light manipulation by dual channel storage in ultra-cold Rydberg medium

Xue-Dong Tian(田雪冬), Zi-Jiao Jing(景梓骄), Feng-Zhen Lv(吕凤珍),Qian-Qian Bao(鲍倩倩), and Yi-Mou Liu(刘一谋)

Chin. Phys. B, 2023, 32 (**4**): 044205. DOI: 10.1088/1674-1056/ac946c

Nonreciprocal negative refraction in a dense hot atomic medium

Hai Yi(易海), Hongjun Zhang(张红军), and Hui Sun(孙辉)

Chin. Phys. B, 2023, 32 (**4**): 044202. DOI: 10.1088/1674-1056/acae7a

Dual-function terahertz metasurface based on vanadium dioxide and graphene

Jiu-Sheng Li(李九生)† and Zhe-Wen Li(黎哲文)

Chin. Phys. B, 2022, 31 (**9**): 094201. DOI: 10.1088/1674-1056/ac5884

Observation of V-type electromagnetically induced transparency and optical switch in cold Cs atoms by using nanofiber optical lattice

Xiateng Qin(秦夏腾), Yuan Jiang(蒋源), Weixin Ma(马伟鑫), Zhonghua Ji(姬中华),Wenxin Peng(彭文鑫), and Yanting Zhao(赵延霆)

Chin. Phys. B, 2022, 31 (**6**): 064216. DOI: 10.1088/1674-1056/ac685a

An analytical model for cross-Kerr nonlinearity in a four-level N-type atomic system with Doppler broadening

Dinh Xuan Khoa, Nguyen Huy Bang, Nguyen Le Thuy An, Nguyen Van Phu, and Le Van Doai

Chin. Phys. B, 2022, 31 (**2**): 024201. DOI: 10.1088/1674-1056/ac2d19

Dynamic light storage based on controllable electromagnetically induced transparency effect

Liu-Ying Zeng(曾柳莹), Jun-Fang Wu(吴俊芳)[†], and Chao Li(李潮)[‡]

School of Physics and Optoelectronic Technology, South China University of Technology, Guangzhou 510640, *China*

(Received 15 November 2022; revised manuscript received 28 April 2023; accepted manuscript online 5 May 2023)

We analytically and numerically investigate a signal light storing mechanism based on the controllable electromagnetically induced transparency (EIT) effect. We demonstrate that the isolation between the waveguide and the cavities cannot be achieved instantly as soon as the two cavities are tuned into resonance, no matter the index tuning rate is ultrafast or slow. We also investigate the temporal evolution features of the intracavity energy when the pulse during time is prolonged. We find many periodical oscillations of the trapped energy in both cavities, and they are entirely complementary. Our analysis shows that the adiabatic wavelength conversion in both cavities and a phase difference π between them play critical roles in this phenomenon.

Keywords: dynamic light storage, electromagnetically induced transparency, dynamic modulation, photonic crystal

PACS: 42.50.Gy, 42.60.Da, 42.70.Qs, 42.82.–m **DOI:** 10.1088/1674-1056/acd2bd

1. Introduction

Signal light storing is of great significance in the fields of photonic circuits, all-optical signal processing and quantum communications.[1–4] The key to realize controllable signal light storing is to greatly slow or stop light. For this purpose, recently, photonic analog of electromagnetically induced transparency (EIT) effect, has been intensively investigated,[5–10] and has been extended to plasmonically induced transparency (PIT) effect.[11,12] The reported slow-light systems using EIT-like effect are mainly based on the static coupling of two or more micro/nanocavities, forming an ultra-narrow EIT peak to ensure slow group velocity.[5–9] However, the ultra-narrow spectral width of EIT peak makes the operating bandwidth quite small, resulting in a delay-bandwidth product limit.[5–9] In order to break this limit, various mechanisms have been proposed.[1,3,13–17] Among them, dynamically tuning the linewidth of EIT peak is a promising method.[5,13,17–21] As has been demonstrated theoretically and experimentally, the linewidth of the supermode, as well as the lifetime of the trapped signal photons, can be freely controlled just by dynamically tuning the resonance difference between the cascaded cavities.[13,21] It is well known that when these resonant frequencies are tuned to be equal, the supermode will be completely isolated from the waveguide. As a result, the previously trapped signal light will be perfectly stored in these cascaded nanocavities.

However, whether or not the isolation between the supermode and the waveguide can be achieved immediately after the cavities are tuned into resonance (i.e., the resonant frequencies of the two cavities are tuned to be equal) is still unknown. This question is rather important, since if the isolation cannot be achieved instantly, part of the signal energy will leak into the waveguide. Obviously, this will affect the storing efficiency. In this paper, we present an analytical model to describe a dynamic light storage system based on the controllable EIT-like effect. From this analytical model, we demonstrate that the supermode cannot be instantly decoupled from the waveguide when we begin to store the signal light. There is always an inevitable, quick, and non-negligible energy leakage, no matter the index tuning rate is fast or slow. We also find the temporal oscillations of intracavity energy when the pulse during time of the signal is prolonged. More importantly, these energy oscillations in the two cavities are entirely complementary. We show that the adiabatic wavelength conversion in both cavities and a phase difference π between them are responsible for this interesting phenomenon.

2. Analytical model

We start by investigating such dynamic processes in a photonic crystal (PC) waveguide-cavities system shown in Fig. 1(a). The structure consists of a triangular lattice of air holes in silicon slab (the refractive index of silicon is $n_0 = 3.4$, and the thickness of the slab is $h = 218$ nm) with a lattice constant of $a = 420$ nm and air-hole radius of $r = 116$ nm. Two monomode nanocavities C_1 and C_2 are side-coupled to a W1 waveguide, which is formed by removing one line of air-holes along the horizon direction. The resonant frequencies of C_1 and C_2 are ω_{01} and ω_{02}, respectively. ω_{01} and ω_{02} are initially slightly different, and can be dynamically tuned via transient nonlinearity, such as free-carrier dispersion effect or

[†]Corresponding author. E-mail: wujf@scut.edu.cn
[‡]Corresponding author. E-mail: lichao@scut.edu.cn

© 2023 Chinese Physical Society and IOP Publishing Ltd

Kerr effect.[13,18–22] For cavity C_i ($i = 1, 2$), the linewidth of the cavity mode is $\gamma_i = \gamma_{Ci} + \gamma_{0i}$, where γ_{0i} and γ_{Ci} originate from the intrinsic cavity losses, and the coupling between the cavity mode and a waveguide, respectively. We suppose the distance between the two nanocavities is far enough, so that their direct coupling can actually be neglected, but they can indirectly couple to each other via the medium waveguide between them.

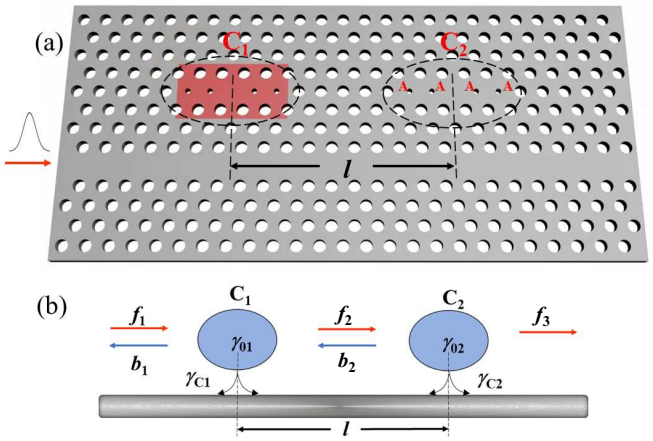


Fig. 1. (a) Dynamic light storage system in a 2D triangular-lattice air-hole PC slab. The refractive index of the red shadowed area is modulated slightly. The physical parameters of C_1 and C_2 cavities are $\omega_{01} = 0.266085$, $\omega_{02} = 0.266201$, $\gamma_{C1} = 3.21 \times 10^{-5}$, $\gamma_{C2} = 3.32 \times 10^{-5}$, and $\gamma_{01} = \gamma_{02} = 8.45 \times 10^{-7}$ (all in units of $2\pi c/a$). (b) Schematic of light storage system consisting of two cavities side-coupled to a waveguide.

Since this linear system is completely reciprocal, we can only consider the forward-transmitted case. According to the temporal coupled-mode theory,[23–25] the dynamic equations for the amplitudes of the cavity modes in C_1 and C_2 can be written as

$$\begin{cases} \mathrm{d}A_1/\mathrm{d}t = (\mathrm{j}\omega_{01} - \gamma_1)A_1 + d_1 f_1 + d_1 b_2, \\ \mathrm{d}A_2/\mathrm{d}t = (\mathrm{j}\omega_{02} - \gamma_2)A_2 + d_2 f_2, \\ f_2 = \mathrm{e}^{\mathrm{j}\phi} f_1 + d_1 A_1, \\ f_3 = \mathrm{e}^{\mathrm{j}\phi} f_2 + d_2 A_2, \\ b_2 = d_2 A_2, \end{cases} \tag{1}$$

where A_i ($i = 1, 2$) is the mode amplitude to represent the electromagnetic energy $|A_i|^2$ stored inside C_i. f_j and b_j ($j = 1, 2, 3$) denote the field amplitudes of the forward and backward transmitted waves at the j-th port in waveguide, as depicted in Fig. 1(b). $d_i = \mathrm{j}\,\mathrm{e}^{\mathrm{j}\phi/2}\sqrt{\gamma_{Ci}}$ is the coupling coefficient between the transmitted waves and the cavity mode of C_i, which can be derived from energy-conservation and time-reversal symmetry constraints (see Appendix A). ϕ stands for the transmission phase, which can be adjusted by changing the distance l between the cavities. As pointed out in several references, ϕ plays an important role not only in EIT systems, but also in PIT systems.[7,26] For instance, Ref. [26] proposed that the properties of a PIT system can be controlled via tuning the resonant phase difference, which is also related to the relative geometrical position of the coupled resonators. Here we choose $\mathrm{e}^{\mathrm{j}\phi} = 1$, which implies a coherent interference between the two cavities. As a result, an EIT-like peak will occur.[13]

To obtain the linewidth of the EIT peak, we should firstly derive the transmission spectrum of the system. This can be done by employing a continuous-wave (CW) probe source $f_1 = \sqrt{p_{\mathrm{in}}}\,\mathrm{e}^{\mathrm{j}\omega t}$ (where p_{in} is the input power, and ω is the carrier frequency) and scanning the wavelength. By substituting this CW source term into Eq. (1) and utilizing the initial condition $A_i(0) = 0$, we obtain the stable total transmission coefficient T as follows:

$$T = \left|\frac{f_3}{f_1}\right|^2 = \left|\frac{(\omega - \omega_{01} - \mathrm{j}\gamma_{01})(\omega - \omega_{02} - \mathrm{j}\gamma_{02})}{[(\omega - \omega_{01}) - \mathrm{j}\gamma_1][(\omega - \omega_{02}) - \mathrm{j}\gamma_2] + \mathrm{e}^{2\mathrm{j}\phi}\gamma_{C1}\gamma_{C2}}\right|^2. \tag{2}$$

When $\phi = m\pi$ (m is an integer), the coherent interference between the two cavities results in a supermode (an EIT-like peak) at $\omega_{\mathrm{EIT}} = (\omega_{01} + \omega_{02})/2$, with a peak transmission of

$$T_{\max} \sim \frac{(\omega_{02} - \omega_{01})^4}{(\omega_{02} - \omega_{01})^4 + 4(\omega_{02} - \omega_{01})^2(\gamma_2 - \gamma_1)^2}. \tag{3}$$

The linewidth (FWHM) of the supermode can be derived by solving

$$\left|\frac{(\omega - \omega_{01} - \mathrm{j}\gamma_{01})(\omega - \omega_{02} - \mathrm{j}\gamma_{02})}{[(\omega - \omega_{01}) - \mathrm{j}\gamma_1][(\omega - \omega_{02}) - \mathrm{j}\gamma_2] + \mathrm{e}^{2\mathrm{j}\phi}\gamma_{C1}\gamma_{C2}}\right|^2 = \frac{T_{\max}}{2}, \tag{4}$$

and we get

$$\Delta_{\mathrm{EIT}} \sim \gamma_{01} + \gamma_{02} + \frac{(\omega_{02} - \omega_{01})^2}{2(\gamma_{C1} + \gamma_{C2})}. \tag{5}$$

From Eq. (5), we know immediately that the coupling rate between the supermode and waveguide is $(\omega_{02} - \omega_{01})^2/[2(\gamma_{C1} + \gamma_{C2})]$, which will vanish when ω_{01} and ω_{02} are tuned to be equal. This means the supermode will be completely isolated from the waveguide. Thus, the previously trapped signal light will be tightly trapped in the two cascaded nanocavities, and the characteristic storing time is determined only by $(\gamma_{01} + \gamma_{02})$.

However, as will be demonstrated below, even if the cavities do not have any intrinsic losses (namely, $\gamma_{01} = \gamma_{02} = 0$), the trapped signal energy cannot be completely stored inside the cascaded cavities. There is an inevitable, quick, and non-negligible energy leakage, which has never been proposed, to the best of our knowledge. To show this more clearly, we consider a signal pulse centered at a carrier frequency ω incident from the left WG. The signal has a Gaussian shape, and takes the form of $f_1 = \sqrt{p_{\mathrm{in}}}\,\mathrm{e}^{\mathrm{j}\omega t} \cdot \mathrm{e}^{-(t-t_{\mathrm{d}})^2/t_0^2}$, where p_{in}, t_0 and t_{d} are the peak power, pulse during time, and delay time of the signal pulse relative to the time origin, respectively.

Initially, the carrier frequency and the during time (so as well as the spectral width) of the signal pulse are appropriately set to match that of the supermode of the EIT-like system. Thus, the signal energy resonantly couples into the supermode

and then reaches a peak. To trap this pulse, the resonance gap between ω_{01} and ω_{02} should be immediately tuned to zero. To do this, we can alternatively keep ω_{02} invariant, and only change ω_{01}

$$\omega_{01}' = \begin{cases} \omega_{02}, & t_1 \le t < t_2, \\ \omega_{01}, & \text{else}. \end{cases} \tag{6}$$

Equation (6) indicates that the signal pulse will be trapped from $t = t_1$ when the supermode is decoupled from the waveguide, and the trapped power will be released at $t = t_2$ after a given storage time.

Considering that the characteristic photon lifetime of the storing process is much longer than the during time of the incident Gaussian pulse, the source term $f_1 = \sqrt{p_{\text{in}}}\,\mathrm{e}^{\mathrm{j}\omega t} \cdot \mathrm{e}^{-(t-t_{\text{d}})^2/t_0^2}$ in Eq. (1) can actually be neglected when t is long enough. Thus, we can derive the analytical solutions of A_1 and A_2

$$A_1(t) = \left[c_1\,\mathrm{e}^{-(\gamma_{\text{C1}}+\gamma_{\text{C2}})t} + c_2\,\mathrm{e}^{-(\gamma_{01}+\gamma_{02})t/2}\right] \cdot \mathrm{e}^{-\mathrm{j}\omega_{02}t}, \tag{7}$$

$$A_2(t) = \frac{\left[c_1\gamma_{\text{C2}}\,\mathrm{e}^{-(\gamma_{\text{C1}}+\gamma_{\text{C2}})t} - c_2\gamma_{\text{C1}}\,\mathrm{e}^{-(\gamma_{01}+\gamma_{02})t/2}\right] \cdot \mathrm{e}^{-\mathrm{j}\omega_{02}t}}{\sqrt{\gamma_{\text{C1}}\gamma_{\text{C2}}}}, \tag{8}$$

where c_1 and c_2 are two undetermined coefficients. Equations (7) and (8) clearly show that the doubly-degenerate modes at ω_{02} have been excited inside the cascaded resonators: one is a low-Q mode, with an energy decay rate of $2(\gamma_{\text{C1}} + \gamma_{\text{C2}})$; another is a high-$Q$ mode, with an energy decay rate of $\gamma_{01} + \gamma_{02}$. Essentially, the generation of the high-Q and low-Q degenerate modes, originates from the destructive/coherent interferences via the waveguide-mediated indirect coupling between the two cascaded cavities, under the condition of $\mathrm{e}^{\mathrm{j}\phi} = 1$. Noticing that $\gamma_{\text{C1}} + \gamma_{\text{C2}} \gg \gamma_{01} + \gamma_{02}$, thus the energy of the excited high-Q mode will be stored inside the cavity, while the energy of the excited low-Q mode will leak into the waveguide. Therefore, there should be a sudden and non-negligible energy dissipation just after the moment when ω_{01} is tuned equal to ω_{02}, with a characteristic dissipation time of $1/2(\gamma_{\text{C1}} + \gamma_{\text{C2}})$. This also means, the isolation between the waveguide and the cavities cannot be achieved instantly as soon as the two cavities are tuned into resonance.

Figure 2 shows the temporal evolution processes of the output waveforms ($|f_3|^2$) for different γ_{C1} and γ_{C2}, by substituting $f_1 = \sqrt{p_{\text{in}}}\,\mathrm{e}^{\mathrm{j}\omega t} \cdot \mathrm{e}^{-(t-t_{\text{d}})^2/t_0^2}$ and Eq. (6) into Eq. (1) and using the four-order Runge–Kutta method[27] to solve these equations. One can see clearly in Fig. 2(a) that a little but non-ignorable dissipation peak occurs just followed closely behind the moment when the modulation begins. When we further increase γ_{C1} and γ_{C2}, we find that the FWHM of the dissipation peak reduces, which indicates that the characteristic time of this sudden energy leakage really varies inversely with $\gamma_{\text{C1}} + \gamma_{\text{C2}}$, as can be seen from Fig. 2(b).

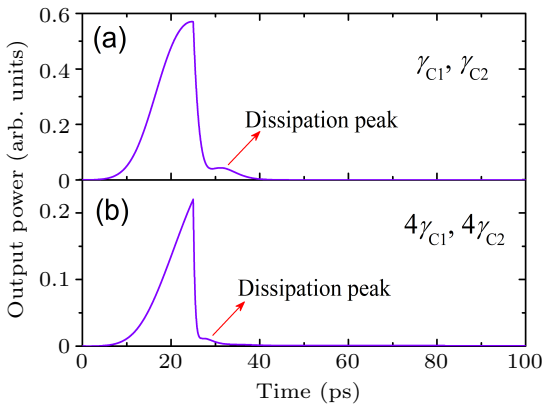


Fig. 2. (a) Energy dissipation in the output waveforms for different γ_{C1} and γ_{C2}. (a) γ_{C1} and γ_{C2} take the original values (see the caption of Fig. 1). (b) γ_{C1} and γ_{C2} increase to 4 times of their original values. One can see that the FWHM of the dissipation peak decreases for bigger γ_{C1} and γ_{C2}.

Next, we will investigate how to control the distribution of the trapped energy inside different cavities on demand, which is of great importance for the applications of controllable optical nonlinearity. Noticing that the term $\mathrm{e}^{-(\gamma_{\text{C1}}+\gamma_{\text{C2}})t}$ can be ignored compared with $\mathrm{e}^{-(\gamma_{01}+\gamma_{02})t}$ when t is long enough (namely, the low-Q mode will decay into the waveguide quickly, while the high-Q mode will preserve inside the resonators), Eqs. (7) and (8) can be further simplified as

$$A_1(t) = c_2\,\mathrm{e}^{-(\gamma_{01}+\gamma_{02})t/2} \cdot \mathrm{e}^{-\mathrm{j}\omega_{02}t}, \tag{9}$$

$$A_2(t) = \frac{-c_2\gamma_{\text{C1}}\,\mathrm{e}^{-(\gamma_{01}+\gamma_{02})t/2} \cdot \mathrm{e}^{-\mathrm{j}\omega_{02}t}}{\sqrt{\gamma_{\text{C1}}\gamma_{\text{C2}}}}. \tag{10}$$

The term $\mathrm{e}^{-(\gamma_{01}+\gamma_{02})t/2}$ in Eqs. (9) and (10) clearly shows that the energy decay rate during the storing process is only determined by the intrinsic losses of the cavities, and the ratio of the trapped signal energy in C_1 to that in C_2 satisfies

$$|A_1(t)|^2/|A_2(t)|^2 = \gamma_{\text{C2}}/\gamma_{\text{C1}}. \tag{11}$$

The relative magnitude of γ_{C1} and γ_{C2} can be readily tuned just by changing the vertical distance between C_1 (or C_2) and the waveguide or the geometry structure of the cavities. Therefore, we can freely control the energy distribution in the cascaded cavities.

To see this more clearly, Fig. 3 shows the theoretically calculated temporal evolutions of the intracavity energy inside C_1 and C_2 during the whole dynamic processes. From Fig. 3, we indeed see that the energy distribution of the trapped signal is sensitive to the ratio of γ_{C1} to γ_{C2}: when $\gamma_{\text{C1}} > \gamma_{\text{C2}}$, more energy is stored in C_2 than in C_1, as shown in Fig. 3(a); while when $\gamma_{\text{C1}} < \gamma_{\text{C2}}$, the result is reversed, as shown in Fig. 3(b); specially, when $\gamma_{\text{C1}} = \gamma_{\text{C2}}$, the energy is equally trapped in both cavities, as shown in Fig. 3(c). More importantly, we find the energy stored in C_i ($i = 1, 2$) is really inversely proportional to its coupling rate $\gamma_{\text{C}i}$, namely, $|A_1|^2/|A_2|^2 = \gamma_{\text{C2}}/\gamma_{\text{C1}}$, just as what Eq. (11) predicts. This conclusion can be tested directly

by measuring the data shown in Fig. 3, e.g., the intersections (marked by red, blue and black dots) of the energy evolution curves and a dashed vertical line at an arbitrary moment of the storing process.

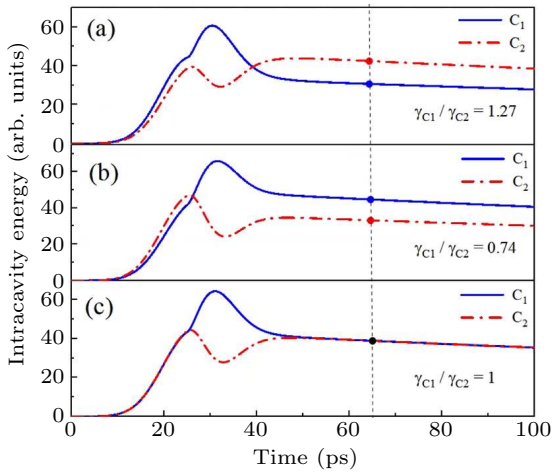


Fig. 3. Temporal evolutions of the intracavity energy with different γ_{C1} and γ_{C2}. (a) $\gamma_{C1} > \gamma_{C2}$. (b) $\gamma_{C1} < \gamma_{C2}$. (c) $\gamma_{C1} = \gamma_{C2}$. The dashed vertical line implies an arbitrary moment of the storing process. In the calculations, $\omega = (\omega_{01} + \omega_{02})/2 = 0.266143\ (2\pi c/a)$, $t_0 = 10$ ps, $t_d = 20$ ps, $t_1 = 25$ ps, $t_2 = 500$ ps, and the others physical parameters are the same as that in the caption of Fig. 1.

3. Numerical experiments

To verify the theoretical predictions of the above analytical model, we use the finite-difference time-domain (FDTD) method[28] to perform numerical experiments on the system sketched in Fig. 1(a). The spatial grids in the horizontal and vertical directions are all chosen to be $a/30$, and the corresponding temporal grid is set to be $0.02(a/c)$. A perfectly matched layer of 1 μm is employed as absorbing boundary. The two nanocavities are created by filling in one air hole, and the radii of the end holes denoted by A are decreased to r_A. Here r_A for C_1 is $0.125a$, while r_A for C_2 is $0.127a$. This slight difference in the size of the end holes makes ω_{01} and ω_{02} detuned initially, with $\omega_{01} = 0.266085\ (2\pi c/a)$ and $\omega_{02} = 0.266201\ (2\pi c/a)$, as shown in the caption of Fig. 1. Besides, the end holes A for both cavities are shifted 42 nm outward from their original positions to increase the vertical radiation Q factors (over 180000). The center distance between the two cavities is tuned to be $l = 13a$ to make sure the propagation phase between C_1 and C_2 satisfies $e^{j\phi} \sim 1$, and the distance is big enough to ignore the direct coupling between the cavities. The vertical distance between the cavity center of C_1 (C_2) and the center line of the W1 waveguide is $4a$. Thus, decay rates of the cavity mode amplitudes for C_1 and C_2 into the W1 waveguide are $\gamma_{C1} = 3.21 \times 10^{-5}\ (2\pi c/a)$ and $\gamma_{C2} = 3.32 \times 10^{-5}$, respectively, corresponding to the coupling Q factors of 4140 and 4000, which are very common in actual PC cavity-waveguide coupling systems.[7] Besides, in real experiments, except for the vertical radiation loss, the PC cavity may also suffer from the scattering/absorption loss. To mimic the real case, here we intensively introduce an imaginary component to the refractive index of C_1 and C_2, with a value of $n_i = 1.43 \times 10^{-6}$, which is equivalent to a cavity intrinsic decay rate of $\gamma_{01}(\gamma_{02}) = 8.45 \times 10^{-7}\ (2\pi c/a)$, corresponding to an unloaded Q factor of 1.57×10^5 for both cavities. Note that under current technology, the cavity intrinsic losses can be well controlled to an extremely low level, and ultrahigh-Q (over 10^6) PC nanocavities have been experimentally realized.[29,30] Therefore, the cavity intrinsic decay rates taken here are reasonable, and can be further decreased by optimal design. When without modulation, the spectrum of the system exhibits a typical EIT peak at $\omega = 0.265945\ (2\pi c/a)$ (or $\lambda_{EIT} = 1548.59$ nm), with a linewidth of $\Delta_{EIT} = 8.43 \times 10^{-5}\ (2\pi c/a)$.

Then, a 10 ps Gaussian signal pulse at $\omega = 0.265945\ (2\pi c/a)$ is injected from the left end of the waveguide, and couples into the cavities efficiently. The pulse during time (or bandwidth) and carrier frequency are selected such that they are coincident with that of the EIT peak. As soon as the trapped signal energy reaches its peak at $t_1 = 25$ ps, we add a fast index modulation of $\Delta n/n_0 = -4.68 \times 10^{-4}$ to C_1, to blueshift ω_{01} and make $\omega_{01} = \omega_{02}$. Here $\Delta n/n_0$ increases linearly from 0 to 8×10^3 within 0.5 ps, which is achievable via the free-carrier dispersion effect or the Kerr effect. Figure 4(a) shows the temporal evolutions of the intracavity energy in C_1 and C_2. After the initial oscillations, the decay rates of the trapped energy in both cavities become very little, with a same value of $1.77 \times 10^{-6}\ (2\pi c/a)$, which corresponds to a characteristic photon lifetime of $\Delta\tau \sim 5.65 \times 10^5 (a/c) = 0.79$ ns. Considering that the operation bandwidth of the system is $\Delta\omega \sim \Delta_{EIT}$, so that the delay-bandwidth product of the system sketched in Fig. 1(a) is $\Delta\omega\Delta\tau \sim 300$, which is far greater than that of a static device (no more than 2π).[5–9] Besides, one might notice that the trapped energy in C_2 (the dashed curve) is less than that in C_1 (the solid curve). That is because γ_{C2} is greater than γ_{C1} (see the detailed parameters in the caption of Fig. 1), and can be well explained according to Eq. (11). Figures 4(c) and 4(e) are the corresponding waveforms of the output signal and the electric field distribution when storing, respectively. One can see clearly that the signal energy is perfectly trapped inside the cascaded cavities.

However, as demonstrated above, the isolation between the waveguide and the cavities cannot be achieved instantly as soon as ω_{01} and ω_{02} are tuned to be equal, since a lossy mode with low Q factor is simultaneously excited during this dynamic process. As a result, part of the trapped signal energy will leak into the waveguide. That is why we see in Fig. 4(c) there is a dissipation peak (with a characteristic time of $1/2(\gamma_{C1} + \gamma_{C2}) \sim 10$ ps) followed closely behind the first transmission peak, just as the theoretically-predicted one

shown in Fig. 2. Note that the characteristic time of this energy dissipation before storing is only determined by γ_{C1} and γ_{C2}, and is nearly independent on the refractive index tuning rate. To verify this, Fig. 5 plots the waveform of the output signal under different index tuning rates (with the tuning time of $\Delta t = 5$ fs, 10 ps, and 20 ps, respectively, as shown by Fig. 5(a)). One can see there is always a little dissipation peak followed by the moment when the index modulation begins, with a nearly same characteristic time, no matter the index tuning is transient or relatively slow.

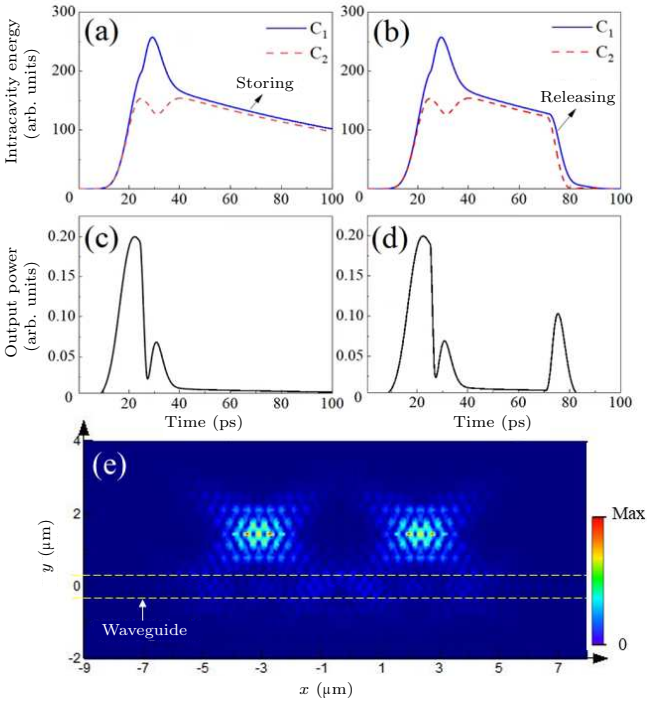


Fig. 4. (a) and (d) Dynamics of the intracavity energy and the output power. In panels (a) and (c), storing starts at $t_1 = 25$ ps. In panels (b) and (d), releasing at $t_2 = 70$ ps. (e) Electric field distribution when storing.

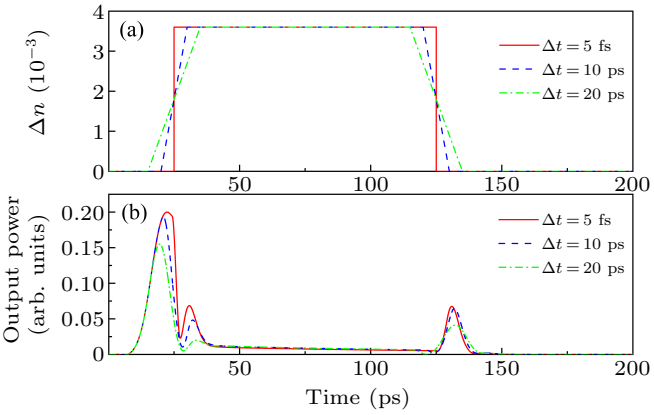


Fig. 5. (a) Refractive index tuning as a function of time. Δt is the index tuning time. (b) Output waveforms under different index tuning rates.

To release the trapped light after a given delay, we can reopen the cavity-waveguide coupling tunnel by adding another fast index modulation to C_1 or C_2, to make their resonances detuned from each other again. As a result, the trapped energy flows out quickly, as shown by Figs. 4(b) and 4(d), as well as Fig. 5. One can see that a pulse appears again, with a quasi-Gaussian shape, nearly independent of the index tuning rate.

Finally, we discuss what will happen when the pulse during time becomes longer. To do this, in the following simulations we consider a signal pulse with longer during time, and all the others parameters, as well as the index modulation (the modulation still stars as soon as the trapped signal energy reaches its peak), are the same as that employed in Fig. 4. From Figs. 6(a) and 6(c), we find more temporal oscillations of intracavity energy appear when the pulse during time is prolonged, with a same oscillation period $\Delta\tau \sim 20.5$ ps. More interestingly, these energy oscillations in C_1 and C_2 seem to be complementary, just as if they were exchanging energy. However, as demonstrated above, the cavities will be completely isolated from the waveguide in 10 ps when a fast index modulation is applied. In addition, the direct coupling of the two cavities can also be ignored due to the long distance between them. That is to say, there is no longer a channel for energy exchange between C_1 and C_2, suggesting that there should be other mechanism at work.

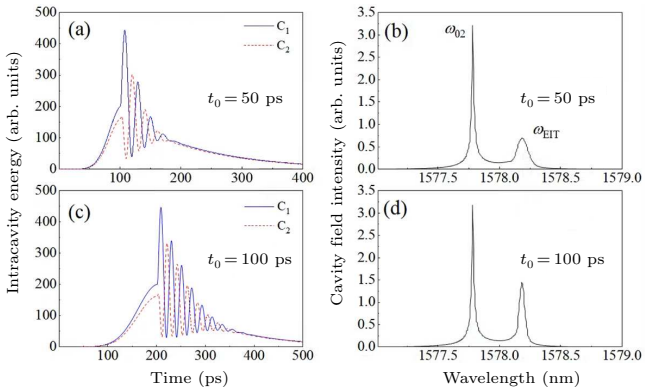


Fig. 6. Temporal and spectral plots of the dynamic storage processes with different pulse during time t_0. (a) and (b) $t_0 = 50$ ps. (c) and (d) $t_0 = 100$ ps.

The intracavity spectra shown in Figs. 6(b) and 6(d) further uncover the truth. We see except for the spectral component of the pump source at $\omega = 0.266135\ (2\pi c/a)$ (or $\lambda = 1578.15$ nm), another new component — the high-Q resonant mode at $\omega_{02} = 0.266201\ (2\pi c/a)$ (or $\lambda_{02} = 1577.71$ nm), is also excited, as predicted by Eqs. (7) and (8). This wavelength shift should be distinguished from the traditional nonlinear cases, since the wavelength conversion is independent of the light intensity. Noticing that this new spectral component is only determined by the final resonance of the dynamically tuned cavity, this wavelength conversion process is essentially adiabatic, just as that reported in Refs. [31–34]. The coexistence of the two components at ω and ω_{02} results in the beat phenomenon in both cavities (the oscillation period $\Delta\tau \sim 20.5$ ps is just equal to $2\pi/|\omega - \omega_{02}|$, which provides a direct evidence[35,36]). More importantly, by comparing Eqs. (7) and (8), the minus sign before the term $e^{-(\gamma_{01}+\gamma_{02})t/2} \cdot e^{-j\omega_{02}t}$ in Eq. (8) implies that there is a phase difference π between the

excited high-Q resonant mode in C_1 and the excited high-Q resonant mode in C_2. That is why the energy oscillations in C_1 and C_2 are complementary. When the energy of the pulse all transfers into the high-Q resonant mode at ω_{02}, these oscillations disappear (see Fig. 6(a) after 200 ps, and Fig. 6(c) after 400 ps).

4. Conclusion

We analytically and numerically investigate a signal light storing mechanism based on the controllable EIT effect. As an example for illustration, we design a compact silicon PC light storing system with two cascaded nanocavities side-coupled to a W1 waveguide. We demonstrate that the isolation between the waveguide and the cavities cannot be achieved instantly as soon as the two cavities are tuned into resonance. We also investigate the case when the pulse during time is prolonged, and find there are many temporal oscillations of light energy inside both cavities with a phase difference π. The underlying physical mechanisms are revealed. These findings may expand our understanding of the dynamic light storage based on the EIT-like effect in a more general framework.

Appendix A

The positions of port 1, port 2, and port 3 are shown in Fig. A1, where port 2 lies at the center between C_1 and C_2, while port 1 and port 3 are symmetrically distributed on both sides of port 2. Thus, the transmission phase between C_1 and C_2 can be written as $\phi = kl$, where k is the waveguide-mode propagation constant, and l is the center-to-center distance between C_1 and C_2. Without loss of generality, here we consider the forward-transmitted case, namely, $b_3 = 0$, and f_1 represents the incident signal light filed.

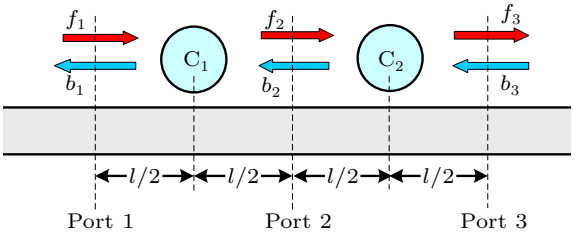


Fig. A1. Schematic of two cavities side-coupled to a waveguide.

In order to determine the coupling coefficients d_1 and d_2 in Eq. (1) and have a better understanding of this equation, we can consider a simplified model by temporally removing the cavity C_2, as shown in Fig. A2. Obviously, the transmitted field f_2 consists of two parts: one is from the incoming wave f_1 through a direct pathway via the waveguide, with a phase difference $\phi = kl$; the other is from the coupling between the transmitted wave and the cavity mode field A_1.

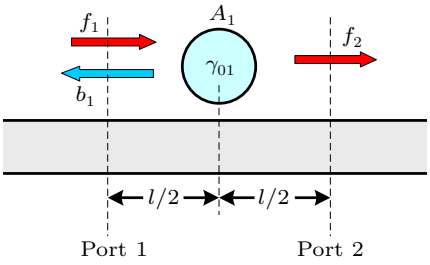


Fig. A2. Schematic of a simplified model.

Accordingly, the transmitted field f_2 can be expressed as

$$f_2 = \mathrm{e}^{\mathrm{j}\phi} f_1 + d_1 A_1. \tag{A1}$$

While the reflected wave b_1 originates directly from the coupling of A_1, and satisfies

$$b_1 = d_1 A_1. \tag{A2}$$

According to the temporal coupled-mode theory,[23] the dynamic equation for the cavity mode field A_1 can be written as

$$\mathrm{d}A_1/\mathrm{d}t = (\mathrm{j}\omega_{01} - \gamma_1)A_1 + d_1 f_1. \tag{A3}$$

From Eq. (A3), we have

$$\mathrm{d}|A_1|^2/\mathrm{d}t = -2\gamma_1|A_1|^2 + d_1 f_1 A_1^* + d_1^* f_1^* A_1. \tag{A4}$$

On the other hand, according to the law of energy conservation, the rate of change of the energy in the resonator mode must satisfies

$$\mathrm{d}|A_1|^2/\mathrm{d}t = |f_1|^2 - |f_2|^2 - |b_1|^2 - 2\gamma_{01}|A_1|^2, \tag{A5}$$

where the terms $|f_1|^2$, $|f_2|^2$, $|b_1|^2$, and $2\gamma_{01}|A_1|^2$ represent the incident power, transmitted power, reflected power, and the cavity intrinsic loss of C_1, respectively. By comparing Eqs. (A4) and (A5), we have

$$\begin{aligned} &-2\gamma_1|A_1|^2 + d_1 f_1 A_1^* + d_1^* f_1^* A_1 \\ &= |f_1|^2 - |f_2|^2 - |b_1|^2 - 2\gamma_{01}|A_1|^2. \end{aligned} \tag{A6}$$

Now, let us perform a time-reversal transformation on the above process. In this case, the flow directions of the energy will all be reversed, and the field terms A_1, f_1, f_2, and b_1 should be rewritten as their conjugations, as shown by Fig. A3.

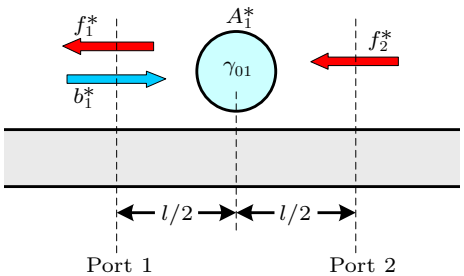


Fig. A3. Schematic of a time-reversal version of the case as shown in Fig. A2.

In this case, we have

$$f_1^* = \mathrm{e}^{\mathrm{j}\phi} f_2^* + d_1 A_1^*. \tag{A7}$$

Taking conjugations on both sides of Eq. (A7), we get

$$f_1 = \mathrm{e}^{-\mathrm{j}\phi} f_2 + d_1^* A_1. \tag{A8}$$

By substituting Eqs. (A2), (A7) and (A8) into Eq. (A6), we obtain

$$|d_1|^2 \cdot |A_1|^2 = (\gamma_1 - \gamma_{01})|A_1|^2 = \gamma_{C1}|A_1|^2. \tag{A9}$$

Accordingly, the coupling coefficient d_1 has the form of

$$d_1 = \sqrt{\gamma_{C1}}\,\mathrm{e}^{\mathrm{j}\theta}, \tag{A10}$$

where θ is a coefficient, and can be further determined by the following means.

By taking conjugations on both sides of Eq. (A1), we get

$$f_2^* = \mathrm{e}^{-\mathrm{j}\phi} f_1^* + d_1^* A_1^*. \tag{A11}$$

Substituting Eq. (A11) into Eq. (A7), we have

$$(\mathrm{e}^{\mathrm{j}\phi} d_1^* + d_1) A_1^* = 0. \tag{A12}$$

Since Eq. (A12) should be satisfied for arbitrary A_1, which means

$$\mathrm{e}^{\mathrm{j}\phi} d_1^* = -d_1. \tag{A13}$$

Substituting Eq. (A10) into Eq. (A13), we immediately obtain

$$\theta = \phi/2 + \pi/2. \tag{A14}$$

Thus, the coupling coefficient d_1 is now completely determined by

$$d_1 = \mathrm{j}\sqrt{\gamma_{C1}}\,\mathrm{e}^{\mathrm{j}\phi/2}. \tag{A15}$$

Similarly, another coupling coefficient d_2 can also be derived as

$$d_2 = \mathrm{j}\sqrt{\gamma_{C2}}\,\mathrm{e}^{\mathrm{j}\phi/2}. \tag{A16}$$

Based on the above-mentioned analysis, it is not difficult to get Eq. (1).

Acknowledgments

Project supported by the National Natural Science Foundation of China (Grant No. 11774098), the Guangdong Natural Science Foundation (Grant Nos. 2022A1515011950 and 2023A1515010781), and the Science and Technology Program of Guangzhou (Grant No. 202002030500).

References

[1] Yanik M F and Fan S 2007 *Nat. Phys.* **3** 372
[2] Otsuka K, Kobayashi N and Tomita M 2007 *Phys. Rev. Lett.* **98** 213904
[3] Yanik M F and Fan S 2004 *Phys. Rev. Lett.* **92** 083901
[4] Stiller B, Merklein M, Wolff C, Vu K, Ma P, Madden S J and Eggleton B J 2020 *Optica* **7** 492
[5] Totsuka K, Kobayashi N and Tomita M 2007 *Phys. Rev. Lett.* **98** 213904
[6] Jiang F, Deng C S, Lin Q and Wang L L 2019 *Opt. Express* **27** 32122
[7] Hu C, Schulz S A, Liles A A and O'Faolain L 2018 *ACS Photon.* **5** 1827
[8] Chai Z, Hu X, Li C, Yang H and Gong Q 2016 *ACS Photon.* **3** 2068
[9] Shen S L, Li J L, Wu J F and Li C 2022 *Eur. Phys. J. Plus* **137** 97
[10] Wang D, Wu J Z and Zhang J X 2016 *Chin. Phys. B* **25** 064202
[11] Guan J, Xia S, Zhang Z, Wu J, Meng H, Yue J, Zhai X, Wang L and Wen S 2020 *Nanoscale Res. Lett.* **15** 142
[12] Xia S X, Zhai X, Wang L L and Wen S C 2018 *Photon. Res.* **6** 692
[13] Xu Q, Dong P and Lipson M 2007 *Nat. Phys.* **3** 406
[14] Tanaka Y, Upham J, Nagashima T, Sugiya T, Asano T and Noda S 2007 *Nat. Mater.* **6** 862
[15] Wang B, Wu J F, Li C and Li Z Y 2018 *Opt. Lett.* **43** 3945
[16] Wu J F, Chen J H and Li C 2022 *New J. Phys.* **24** 053005
[17] Mario L Y and Chin M K 2008 *Opt. Express* **16** 1796
[18] Liu Y C, Li B B and Xiao Y F 2017 *Nanophotonics* **6** 789
[19] Zheng C, Jiang X, Hua S, Chang L, Li G, Fan H and Xiao M 2012 *Opt. Express* **20** 18319
[20] Elshaari A W, Aboketaf A and Preble S F 2010 *Opt. Express* **18** 3014
[21] Xu Z M, Li C and Wu J F 2020 *New J. Phys.* **22** 063030
[22] Zhao Y, Zhang Y N, Wang Q and Hu H 2015 *IEEE Trans. Nanotechnol.* **14** 407
[23] Fan S, Suh W and Joannopoulos J D 2003 *J. Opt. Soc. Am. A* **20** 569
[24] Li C, Wang M and Wu J F 2017 *Opt. Lett.* **42** 334
[25] Maes B, Bienstman P and Baets R 2005 *J. Opt. Soc. Am. B* **22** 1778
[26] Xia S X, Zhai X, Wang L L, Xiang Y J and Wen S C 2022 *Phys. Rev. B* **106** 075401
[27] Iserles A 1996 *A First Course in the Numerical Analysis of Differential Equations* (Cambridge: Cambridge University Press)
[28] Taflove A and Hagness S C 2000 *Computational Electrodynamics* (Boston: Artech House)
[29] Ashida K, Okano M, Ohtsuka M, Seki M, Yokoyama N, Koshino K, Mori M, Asano T, Noda S and Takahashi Y 2017 *Opt. Express* **25** 18165
[30] Kuramochi E, Grossman E, Nozaki K, Takeda K, Shinya A, Taniyama H and Notomi M 2014 *Opt. Lett.* **39** 5780
[31] Notomi M and Mitsugi S 2006 *Phys. Rev. A* **73** 051803
[32] Preble S, Xu Q and Lipson M 2007 *Nat. Photon.* **1** 293
[33] Preble S, Cao L, Elshaari A, Aboketaf A and Adams D 2012 *Appl. Phys. Lett.* **101** 171110
[34] Chen J H, Zhang Y B, Li C and Wu J F 2022 *Results Phys.* **40** 105796
[35] Wu J F and Li C 2014 *Opt. Lett.* **39** 5271
[36] Li C and Wu J F 2015 *IEEE Photon. J.* **7** 6500408